RESEARCH ARTICLE

DOI: 10.54392/irjmt26218

Asian Research Association

INTERNATIONAL RESEARCH JOURNAL OF MULTIDISCIPLINARY TECHNOVATION

Vitis Vinifera Assisted Synthesis of Isotropic NiO Nanoparticles: Investigation of Physicochemical Properties for Antibacterial and Anticancer Activities

N. Backiyalakshmi [a, *], G. Magesh [b], S. Sindhu Kavi [c], E. Ranjith Kumar [c], M. Deepty [d], Vinayakprasanna N. Hegde [e], G. Venkata Rao [f], Ch. Srinivas [d], A. Ramalingam [g, *]

[a] Department of Science and Humanities, KGiSL Institute of Technology, Coimbatore 641035, Tamil Nadu, India
[b] Department of Physics, Thiruvalluvar College, Papanasam, Tirunelveli 627425, Tamil Nadu, India.
[c] Department of Physics, KPR Institute Engineering and Technology, Coimbatore 641407, Tamil Nadu, India
[d] JNTU-Kakinada Research Centre, Nanomaterials and Nanomagnetism Research Laboratory, Department of Physics, Sasi Institute of Technology & Engineering, Tadepalligudem 534101, Andhra Pradesh, India
[e] Department of Physics, Vidyavardhaka College of Engineering, Mysuru-570002, Karnataka, India
[f] Department of Science and Humanities, University College of Engineering, Adikavi Nannaya University, Rajamahendravaram 533296, Andhra Pradesh, India.
[g] Department of Physics, Government Arts College, Udumalpet- 642126, Tamilnadu, India
* Corresponding Author Email: priasumi@gmail.com , ramligri75@gmail.com

DOI: https://doi.org/10.54392/irjmt26218
Received: 04-01-2026; Revised: 16-03-2026; Accepted: 21-03-2026; Published: 30-03-2026

Abstract: Nickel oxide nanoparticles (NiO NPs) have been synthesised through a green combustion method, employing *Vitis vinifera* as a facilitating agent. The synthesised NiO nanoparticles undergo thermal treatment within the temperature range of 350°C to 450°C. This study delves into the physicochemical properties and biological applications of NiO nanoparticles that have undergone specific thermal treatment conditions. The XRD patterns demonstrated the presence of cubic Ni/NiO phases. The experimentally determined lattice parameter for the NiO phase is observed to lie within the range of 4.1737 to 4.1783 Å, whereas for the Ni phase, it is found to be between 3.5241 and 3.5280 Å. The observed variation in crystallite size indicates the occurrence of Ostwald ripening. The typical crystallite size for the NiO phase ranges from 21.2 to 22.1 nm, whereas for the Ni phase, it spans from 45.8 to 33.2 nm. The thermogravimetric analysis (TGA) and differential thermal analysis (DTA) demonstrated the thermal stability of NiO nanoparticles, as well as the effects of heat treatment. The values for Young's modulus (Y), rigidity modulus (G), and bulk modulus (B) are approximately 122, 44, and 178 GPa, respectively. The investigation reveals that the elastic moduli exhibit an increase with the progression of sintering. The derived value of Poisson's ratio (σ) at 0.385 suggests that the samples, both as-prepared and sintered, exhibit isotropic and compressible characteristics. The B/G ratio for both the as-prepared and sintered samples is approximately 4, suggesting a ductile characteristic inherent in the samples. The vibrational spectra of heat-treated NiO nanoparticles were subjected to analysis through Fourier-transform infrared spectroscopy. The structural morphology of the samples exhibiting agglomeration is elucidated through FE-SEM micrographs. Moreover, the particle dimensions obtained via TEM correspond with the fluctuations in crystallite size observed following thermal treatment. The assessment of the antibacterial characteristics of green synthesised NiO nanoparticles was carried out against both gram-positive and gram-negative bacterial pathogens. Research into antibacterial properties has demonstrated that NiO nanoparticles synthesised via green combustion exhibit significant efficacy in suppressing bacterial proliferation. The research examined the possible cytotoxic impacts of NiO nanoparticles synthesised via green combustion on the A549 lung cancer cell line. The results demonstrate that the synthesised NiO nanoparticles display a toxicity effect on the A549 cancer cell line that is dependent on the dosage administered.

Keywords: Nanomaterials, Green Combustion Synthesis, Structural Analysis, Elastic Behaviour, Microstructure, Antibacterial and Anti-Fungal Activities.

1. Introduction

Large-scale industrial development has led to significant economic growth. On the other hand, environmental degradation is unavoidable due to various pollutions of which major contributions are from water and air pollutions. The harmful bacteria developed due to these pollutions are causing several health problems and skin diseases. To get rid of these problems, several antibiotics are serving in the form of pills for easier consumption. Apart from these antibiotics, metal oxides like ZnO, MnO, Fe_3O_4, Co_3O_4 have been tested for antibacterial activity due to their antioxidant properties. Among various metal oxides, nickel oxide (NiO) is of special interest due to its stability and excellent optoelectronic properties. Generally, NiO is anti-ferromagnetic exhibiting p-type semiconducting behaviour with a large band gap ranging from 3.4 to 4 eV [1, 2]. Owning to its electronic structure and chemical bonding an interesting electrical behaviour is associate with the NiO. It is broadly recognized as an insulator characterized by charge-transfer and another type of Mott Hubbard insulator characterized by a wide energy gap [3, 4]. The wide band gap has limited its optoelectronic properties. To enhance the physiochemical properties, various metals and non-metals are incorporated in the host lattice. Apart from these modifications, the retreat of NiO under nanoscale dimensions tuned its properties for wide range of applications.

Nickle oxide nanoparticles (NiO NPs), prone to have large surface area, flexible bandgap, exceptional thermal durability and potent catalytic behavior. Due to these features, nanoparticles made of NiO can be used in many kinds of fields such as medical science, storage of energy, catalytic activity, and gas sensors [5]. Among their potential interesting applications, NiO NPs show potential for their effectiveness as antibacterial and antifungal agents, suggesting an innovative approach towards biocidal activity and solving an increasing issue of resistance to antibiotics [6]. Thermal combustion approach, a simple budget-friendly and sustainable synthesis approach for synthesizing NiO NPs with controllable size, shape, and crystallinity. In order to produce sufficient oxide nanoparticles, this process involves an oxidant and a fuel that require an exothermic chemical reaction. for large-scale production, the thermal combustion approach is remarkable to generate crystalline nanoparticles with a low energy input along with rapid reaction times. Additionally, this technique can be improved by adding dopants or change surface properties to improve the biocidal activity of NiO NPs [7-10].

Incorporating natural components into the synthesis of nanoparticles has evolved into an environmental and sustainable method that corresponds with both budget-friendly and environmental beneficial targets [11]. In such an instance, Fruit juice's abundant collection of biomolecules, including glucose, phenolic chemicals, alkaline compounds, and flavonoids that are makes it an exceptional natural capping and stabilizing component. Through prohibiting agglomeration and modifying the size and structure of the nanoparticles, these biomolecules stabilize the particles in addition to facilitating with reducing the amount of metal ions. The technique is additionally more beneficial to the environment since grapes juice is utilized instead of harmful and hazardous chemicals [12-14]. Khan *et al.* [15], synthesized NiO NPs utilizing onion extracts. A comparison was made between the impact of quercetin and onion extracts. The comparison research yielded nearly identical results. The antibacterial efficacy of these NiO NPs was assessed. Ahmad *et al.* [16], produced NiO NPs utilizing aloe Vera gel extract. The researchers investigated the impact of annealing on NiO NPs. The antimicrobial experiments were conducted to evaluate the effectiveness against both gram-positive and gram-negative bacteria. Sadhukhan *et. al* [17], compared the properties of reduced graphene oxide and NiO NPs that were synthesized utilizing guava leaf extract by a phytochemical technique. Haider *et al*. [18], conducted a study where they used ginger and garlic extracts to create NiO NPs through a green synthesis method. The researchers then evaluated the antibacterial and photocatalytic properties of the samples generated. According to their research, chemically manufactured nanoparticles can be used instead of green created nanoparticles in industrial applications.

The present research aims to synthesis NiO NPs through grape fruit juice assisted green thermal combustion method. The synthesized NiO NPs were thermally treated at different temperatures at 350°C and 450°C. The development of nanoparticles with improved crystallinity, consistent shape, and functionalized surfaces is ensured using the green thermal combustion method in connection with the biogenic characteristics of grapes juice. The impact of annealing treatment on the antibacterial activity and physicochemical characteristics of NiO NPs was thoroughly examined. The antibacterial and antifungal efficacy of these naturally occurring NiO nanoparticles against different infectious strains was evaluated. In order to understand the mechanism of action, which involves the rupture of cell membranes and the production of oxygen species that are reactive (ROS), the combined effects of the phytochemicals from the grape juice and the naturally occurring antimicrobial properties of NiO nanoparticles are investigated. The impact of annealing treatment on the antibacterial activity and physicochemical characteristics of NiO NPs was thoroughly examined.

2. Experimental procedure

2.1 Methods and Materials

A green combustion technique has been employed to synthesize the metal oxide nanoparticles. This process efficiently oxidizes metal nitrates. 1M of Nickel nitrate hexahydrate Ni $(NO_3)_2 \cdot 6H_2O$, which is of high purity and suitable for analysis, underwent thermal decomposition to produce nanoparticles of Nickel oxide. The combustion reaction was initiated using 50ml of freshly extracted grape fuel. At first, a solution containing 1M of Nickel nitrate was combined with 50 ml of distilled water using a magnetic stirrer. 50 ml of grape extract is introduced into the solution and agitated consistently for a duration of 1 hour. The solution is maintained on the hotplate at a temperature of 100°C. Ultimately, the process of burning occurs, resulting in the formation of metal oxide, which is then gathered as ash and finely pulverized into nanoparticles. In addition, the manufactured samples were subjected to heat treatment at temperatures of 350°C and 450°C. A comparative analysis was conducted to examine the impact of heat treatment. The physicochemical parameters of the samples were analyzed using various characterization techniques.

2.2 Characterization Techniques

The structural characteristics of NiO NPs were investigated using XRD (Bruker AXS D8 diffractometer, CuKα wavelength 1.5406Å). The surface morphology and elemental analysis were investigated with a Zeiss Gemini 300 FESEM and TEM (JEM-2100 Plus). Thermal measurements were conducted using TG-DTA research (Perkin Elmer). Shimadzu's IR Tracer 100 was used to conduct FTIR study on the vibrational modes and functional groups found in NiO NPs. The antibacterial and antifungal characteristics of NiO NPs were examined using the agar well diffusion method [19].

3. Results and discussion

3.1 Structural Analysis

X-ray diffraction (XRD) was examined to investigate the crystallite size and phase characteristics of the green thermal combustion synthesized NiO NPs. Figure.1 displays the Rietveld refined XRD patterns of as-prepared and sintered NiO NPes. The Rietveld refined was performed by Profex software. The fundamental parameters approach (FPA) was considered for profile calculation. The reliability factors (R_{wp} and R_{exp}), goodness of fit (GoF) and chi-square (χ^2) are listed in Table.1. The refinement was performed by iteratively fitting a calculated pattern to the experimental (observed) data. This was attained by adjusting key parameters such as crystallite size, strain and lattice constants. The refinement process continued until an acceptable goodness of fit (GoF) and chi-square (χ^2) values were achieved. As shown in the Figure.1, the observed and calculated patterns are well matching with each other with minimal difference. This indicates the successful Rietveld refinement of XRD profiles. The GoF and χ^2 are around one for all samples. The indexed diffraction peaks (111), (200), (220), (311) and (222) are related to the NiO phase and are consistent with the JCPDS card number 00-047-1049. The peaks (111), (200) and (220) marked with asterisk are related to Ni phase and are consistent with JCPDS card number 87-0712. The crystal structure of both the phases is of face centered cubic (FCC) belonging to Fm-3m space group. Similar reports can be found in the literature [20]. The present metal oxide nanoparticles consist of both NiO and Ni NPs. The presence of such an existence of NiO/Ni NPs can be expected due to the nature of combustion reagent grape juice used in the present green synthesis method. Generally, grape juice is in rich of tartaric (75%) and citric (25%) acids. Both these acids probed the combustion reactions for the formation of NiO and Ni NPs. When nickel nitrate solution was mixed with grape juice, metal nitrate solution undergone redox reaction for combustion with both tartaric and citric acids. The formation of major portion NiO NPs can be expected from the redox reaction of tartaric acid and the creation of Ni NPs can be anticipated due to redox reaction of citric acid. The possible reaction mechanisms for the formation of Ni and NiO NPs are.

$$Ni(NO_3)_2 6H_2O + C_4H_6O_6 \text{ (Tartaric acid)} \rightarrow NiO + 9H_2O + 4CO_2 + N_2 \quad (1)$$

$$Ni(NO_3)_2 6H_2O + C_6H_8O_7 \text{ (Citric acid)} + 3/2O \rightarrow Ni + 6H_2O + 6CO_2 + N_2 \quad (2)$$

The formation of Ni NPs from the redox reaction of citric acid may be due its easier combustion with oxygen compared to the tartaric acid. The experimental lattice parameter (*a*) has been evaluated using powder indexing programme. The characteristics of diffraction peaks are used to evaluate average crystallite (*D*) from the Scherrer formula [21].

$$D = \frac{k \cdot \lambda}{\beta \cos\theta} \quad (3)$$

Table 1. Rietveld refinement parameters.

Sample	R_{wp}	R_{exp}	*GoF*	χ^2
As prepared	3.04	2.80	1.09	1.18
350°C	3.15	2.83	1.12	1.18
450°C	3.19	2.81	1.14	1.20

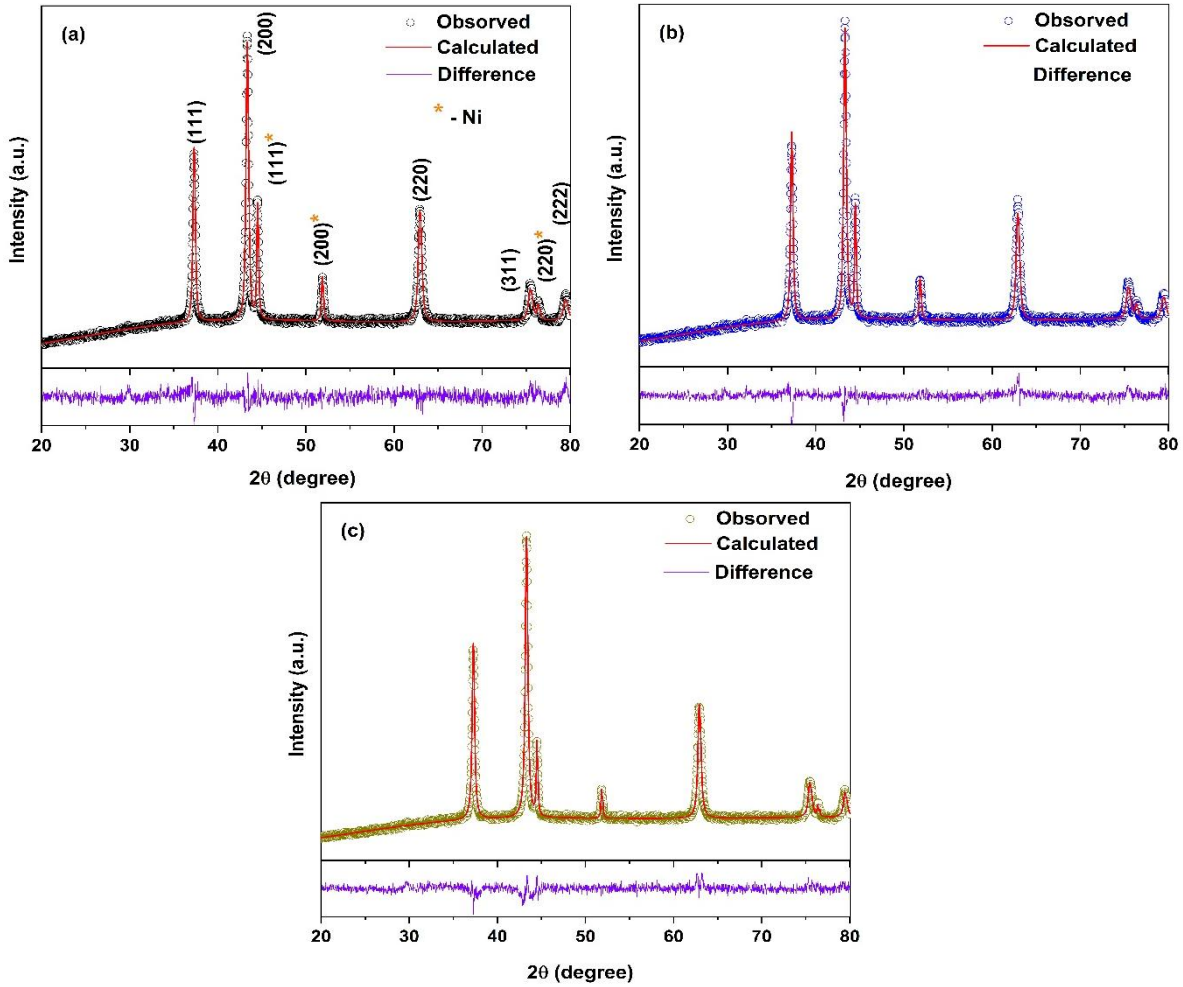

Figure 1. Rietveld refinement of XRD patterns of as-prepared and sintered NiO samples: **(a)** as-prepared, **(b)** 350oC and **(c)** 450oC.

Table 2. Structural parameters of Ni/NiO phases.

sample	NiO phase		Ni phase	
	a (Å)	*D* (nm)	*a* (Å)	*D* (nm)
As-prepared	4.1737	21.2	3.5241	45.8
350°C	4.1746	21.3	3.5265	34.7
450°C	4.1783	22.1	3.5280	33.2

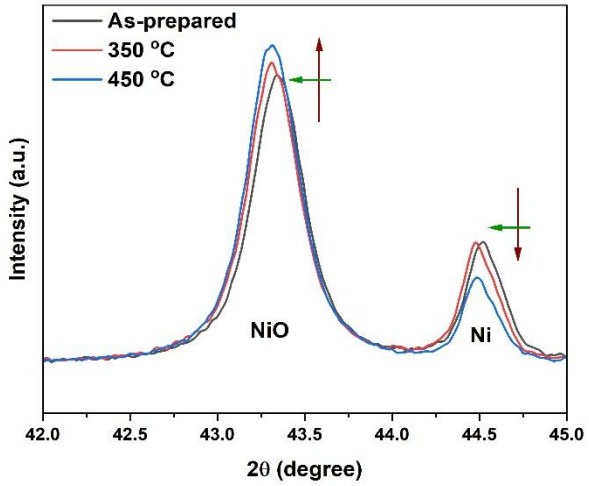

Figure 2 Variation of intensity of NiO and Ni phases with 2θ.

The evaluated values of *a* corresponding to NiO and Ni phases along with their average crystallite sizes are listed in Table 2. It was observed that the value of *a* related to NiO phase is increasing with sintering temperature. Interestingly, the value of *a* corresponding to Ni phase is also in the increasing trend with the sintering temperature. Such a variation of experimental lattice parameter of NiO and Ni may be attributed to transformation of Ni phase into NiO phase at elevated temperatures. The variation of intensity of prominent peaks of NiO and Ni phases with 2θ is shown in Figure.2. It can be clearly observed that the value diffraction angle is shifting towards the lower value with sintering temperature in both NiO and Ni phases. It is ascribed to the increase in experimental lattice parameter supporting the evaluation of *a* from the Powder index programming.

It can be fairly observed from the intensity of diffraction peaks of NiO phase is increasing while it is decreasing for Ni phase with the sintering temperature. Moreover, the broadening of NiO phase is decreasing while it is increasing for Ni phase with the sintering temperature. Such changes in intensity and broadening attributes to the change in crystallite sizes. The mean size of the crystallites in the freshly synthesized NiO NPs is 21.2 nm. An increase in temperature leads to an increase in the size of the crystallites. At temperatures of 350°C and 450°C, the sizes of the crystallites are observed to be 21.3 nm and 22.1 nm respectively. The crystallite size of Ni phase is found to be 45.8 nm, 34.7 nm and 33.2 nm. The typical variation of crystallite size observed in Ni Phase can be expected due to phase transformation into NiO phase. The phase transformation will be identified from thermogravimetric analysis.

3.2. Thermal Analysis

The thermogravimetric analysis (TGA) and differential thermal analysis (DTA) curves of the nickel oxide nanoparticles were presented in Figure.3 (a-c). In Figure.4a, there are two distinct weight losses observed in TGA curves: one occurring at 63.3°C and another at 506.5°C. The initial weight loss observed at 68.5°C and 65.2°C for the annealed NiO NPs. Water desorption is responsible for the slight weight losses reported at temperatures ranging from 63°C to 68°C. The second weight loss was found to be between 720°C and 730°C for annealed NiO NPs (see Figure3b & Figure.3c). The second weight loss observed between 720°C and 720°C is ascribed to NiO impurities or adsorbents. In addition to the decrease in weight, there are two distinct DTA peaks observed at temperatures between 123.1°C to 135.2°C and 465.65°C to 490°C. The weight losses are associated with the depletion of oxygen, resulting in the formation of oxygen vacancies. The weight loss is a result of the heat breakdown of NiO NPs. It can be observed that the no further weight loss was observed above 750ºC. As anticipated in the XRD studies, the complete phase transformation into NiO phase is taking place at elevated temperatures. Since the sample is sintered at 350 and 450ºC which is below 750ºC, we are observing the both Ni/NiO phases.

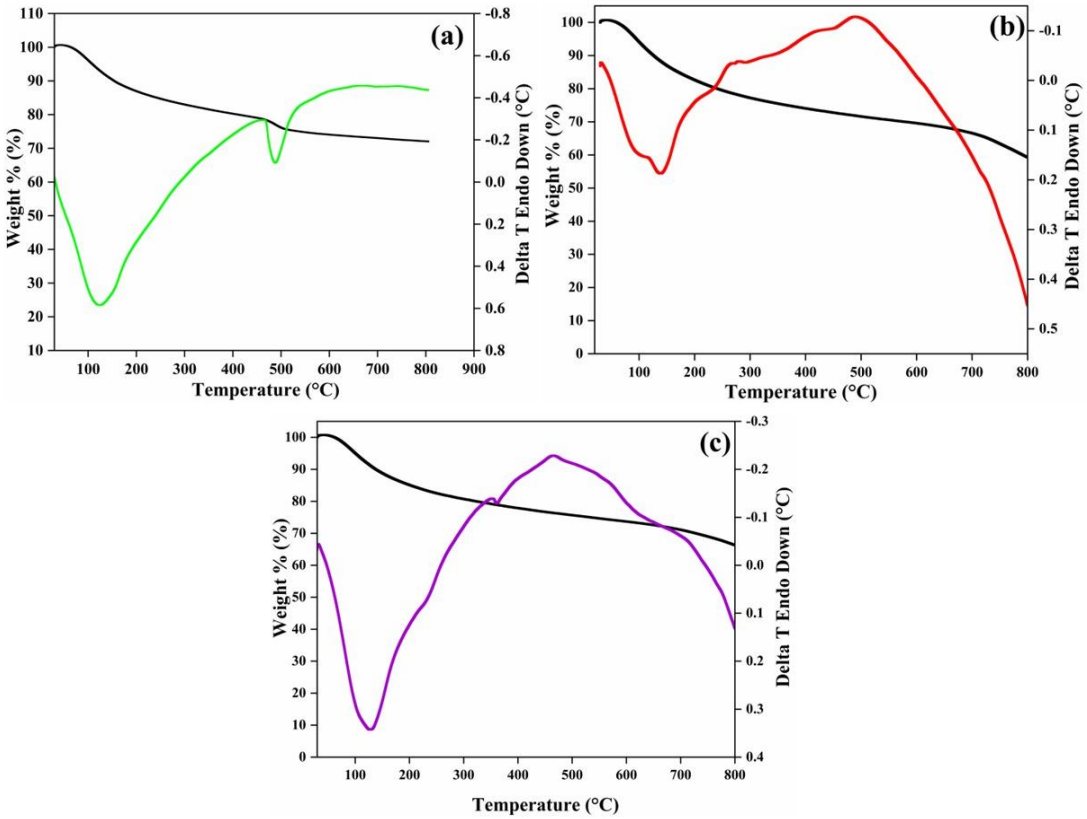

Figure 3. Thermal analysis of as-prepared and sintered NiO NPs **(a)** as-prepared, **(b)** 350℃ and **(c)** 450℃.

At high sintering temperatures, Ni oxidized with the oxygen and transformed into NiO phase. The argument supported with decrease of intensity of diffraction peaks of Ni phase with the rise in temperature. Such that the Ni phase is allowed to dissolve with NiO phase at elevated temperature.

3.3 Elastic studies

Elastic parameters like Young's modulus (*Y*), bulk modulus (*B*), shear modulus (*G*) and Poisson's ratio (*σ*) are very useful to understand the mechanical properties of a material. The elastic moduli (E_{hkl}) have been evaluated based on the Hook's law [22]. Elastic constants and moduli were determined using the CASTEP module using generalized gradient approximation (GGA) with the Perdew–Burke–Ernzerhof (PBE-Sol) exchange–correlation functional.

This approach allows reliable prediction of Young's (*Y*), shear (*G*) and bulk (*B*) moduli as well as Poisson's ratio (*σ*) and elastic anisotropy. Table 3, provides the calculated elastic properties using Voigt approximation. The elastic behaviour of a material whether it is brittle or ductile can be known by the ratio of bulk modulus (*B*) to rigidity modulus (*G*) proposed by Pugh [23]. The characteristic value of *B*/*G* to differentiate between brittle and ductile nature is 1.75. Based on the value of *B*/*G*, the material is brittle for a value less than 1.75 and it is ductile for a value greater than 1.75. The value of *B*/*G* for the as-prepared and sintered NiO NPs is greater than 4 than can be noted from the Table 3. It attributes that the present NiO NPs are more ductile nature possessing excellent mechanical stability.

The three-dimensional representations of *Y*, *G* and *σ* shown in the Figure.4 for the as-prepared and thermally treated samples. As shown in the Figure 5, the nearly spherical shape of the 3D surfaces suggests a predominantly isotropic elastic response, with only minor deviations. For the as-prepared nanoparticles, Young's modulus (*Y*) is calculated to be 122.10 GPa, shear modulus 44.06 GPa, bulk modulus 178.04 GPa and Poisson's ratio of 0.385. These values indicate a mechanically stable system with significant ductility, as reflected by the relatively high Poisson's ratio. Upon sintering at 350°C and 450°C, the elastic parameters such as *Y*, *G*, *B* and σ exhibited a slight increase. These increments indicates that thermal treatment enhances structural densification without drastically altering the intrinsic mechanical rigidity of the system. Notably, the anisotropy factors remain very close to unity (ranging from 1.025 to 1.033) for all parameters of all samples, confirming that the material retains near-isotropic elastic behaviour across different processing conditions. The high *B* values coupled with consistent *G*, confirms strong interatomic bonding within the system, conferring resistance to volume change and shear deformation. The stable *σ* across all samples indicates that the ductile nature of the material is preserved even after heat treatment.

3.4 Vibrational Analysis

The vibrational properties of the NiO NPs were analyzed over the spectral range of 4000 to 400 cm^{-1} by KBr pellet approach. The FTIR spectra of as-prepared and sintered sample is shown in Figure 5. The FTIR analysis identifies the presence of various organic compounds present in the given sample. Thus, the vibrational characteristics of the NiO NPs prepared using Vitis vinifera were examined. NiO NPs transmitted spectra have been identified between 450 and 3700 cm^{-1}. The production of NiO NPs is confirmed by the peak shift from 486.06 cm^{-1} to 509.21 cm^{-1}. In addition to the analogous band vibrations and visible shifting in peaks of the NiO NPs result justifies that the natural components present in the grape extract is responsible for the capping and reduction process. The existence of C=C alkenes is indicated by bending vibrations detected at 864.11 cm^{-1}, 879.54 cm^{-1}, and 871.82 cm^{-1}. According to the peaks at 1458.18 cm^{-1}, 1450 cm^{-1} and 1481 cm^{-1} there may be hydroxyl groups or water molecules present. The O–H stretching mode of hydroxyl groups is also shown by the peaks at 3678.41 cm^{-1}, 3695.61 cm^{-1} and 3379.29 cm^{-1}. The increase in particle size with temperature is responsible for the observed shift in the transmission spectra, and XRD analysis provides additional support for this theory.

Table 3. Elastic properties of as prepared and sintered samples.

Sample	*Y* (GPa)	*G* (GPa)	*B* (GPa)	*σ*	*B/G*
As prepared	122.10	44.06	178.04	0.385	4.040
Anisotropy	1.029	1.033	-	1.0589	
350°C	122.22	44.09	178.07	0.385	4.039
Anisotropy	1.03	1.027	-	1.0565	
450°C	122.35	44.13	178.24	0.385	4.039
Anisotropy	1.025	1.031	-	1.0495	

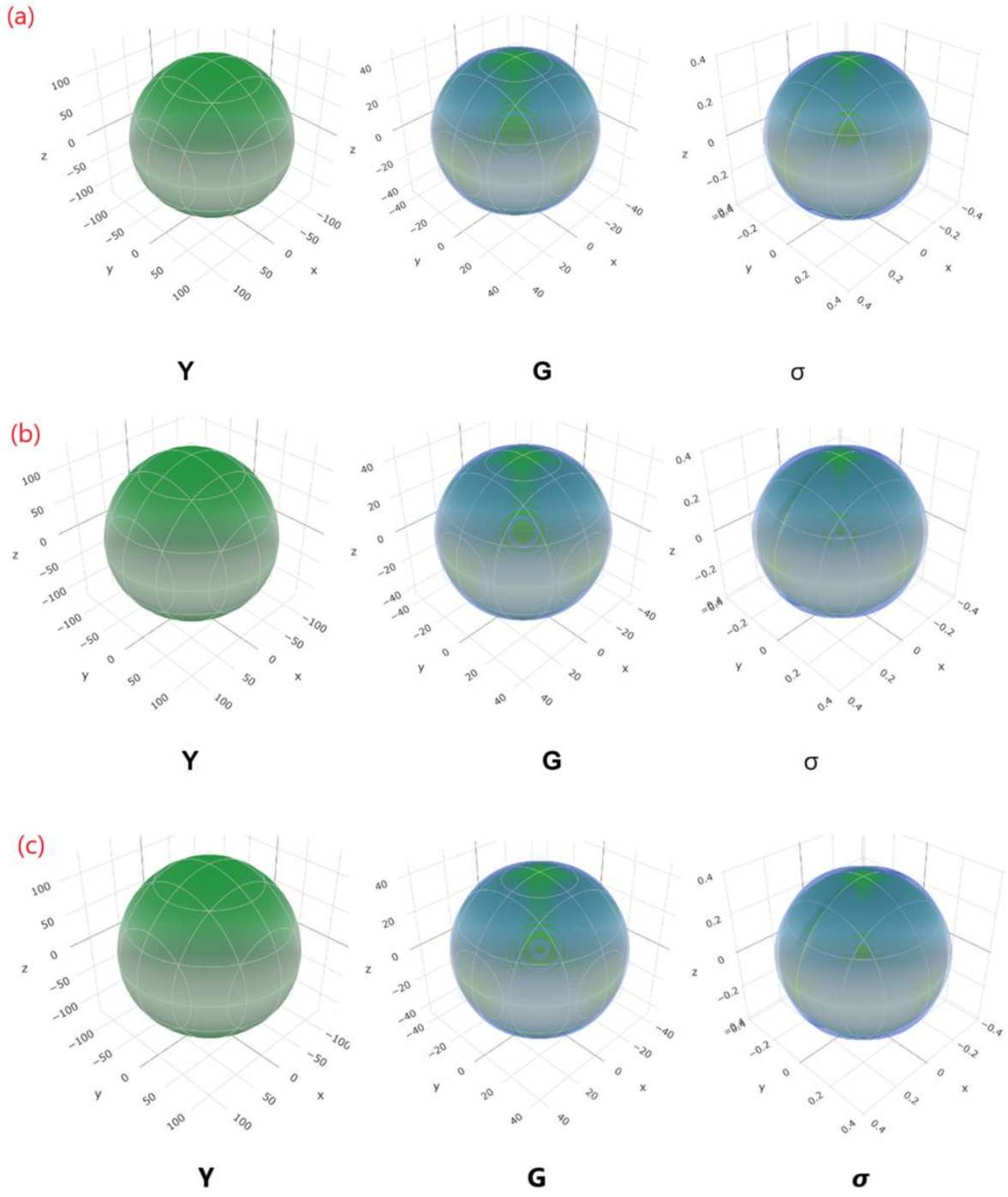

Figure 4. Young's modulus (Y), shear modulus (G) and Poisson's ratio (σ) of (a) as prepared, (b) 350oC and (c) 450oC sintered nanoparticles

3.5 FE-SEM and TEM analysis

The surface morphology is usually analyzed using SEM. This electron microscopy method gives the 10^6x magnified image of the surface present. Figure.6 shows the surface morphology of the prepared NiO NPs. The agglomerations of the NiO NPs were observed for the prepared sample. In the sintered samples, the slight disappearance of the agglomeration is intensified. Similar results can be found the literature [24, 25]. The occurrence of porous structure is likely present. NiO NPs heated at 450°C shows a clear porous structure. Figure.7 depicts the TEM and SAED patterns of NiO NPs generated utilizing the natural juice assisted green combustion approach. The TEM images confirm the exterior shape acquired from FESEM, and the particle sizes are consistent with the crystallite size obtained from XRD. The average particle size of the as-prepared NiO NPs is 23.4 nm, but the annealed NiO NPs exhibit an improved crystalline nature with larger particle sizes than the as-prepared NPs.

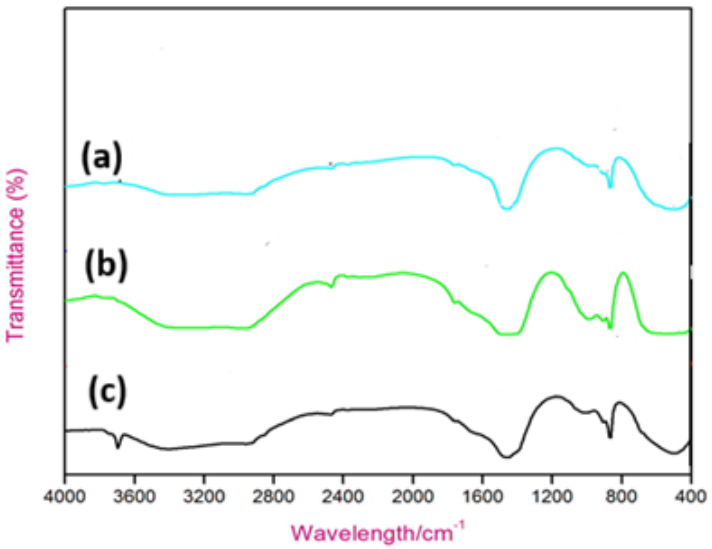

Figure 5. Vibrational spectra of as-prepared and sintered NiO NPs: **(a)** as-prepared, **(b)** 350℃ and **(c)** 450℃.

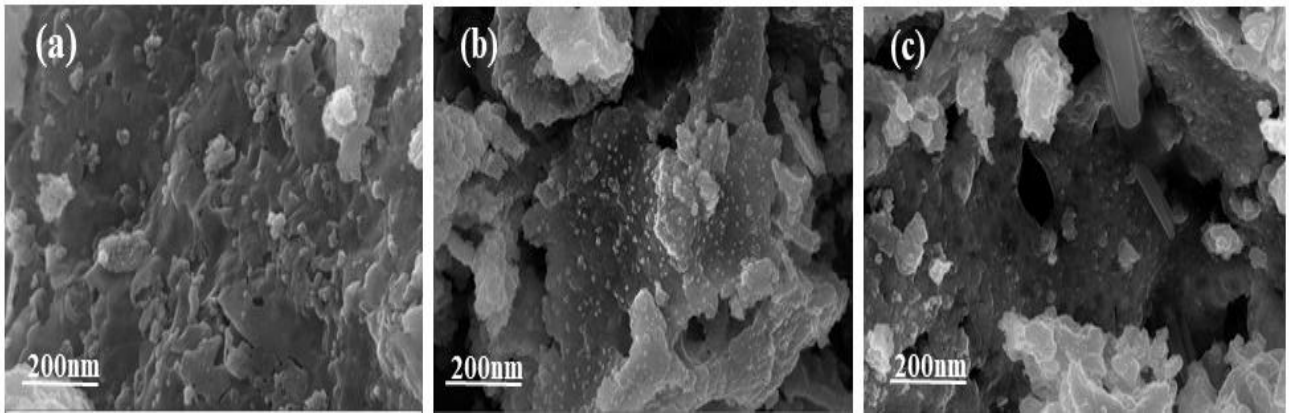

Figure 6. Surface morphology of as-prepared and sintered NiO NPs: **(a)** as-prepared, **(b)** 350℃ and **(c)** 450℃.

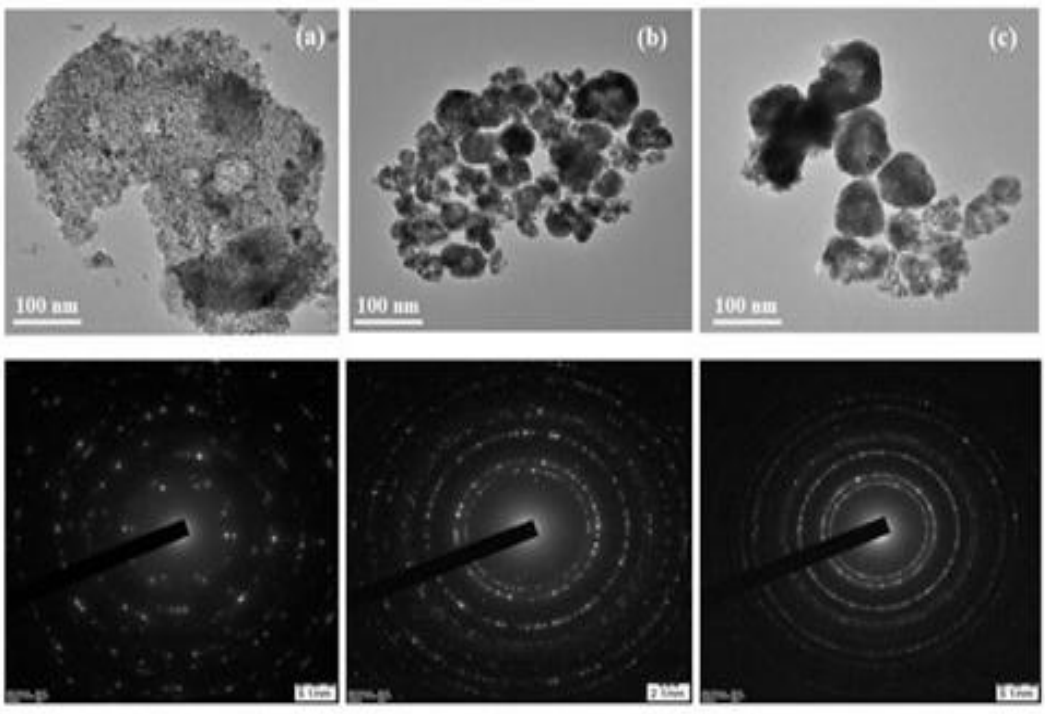

Figure 7. TEM and SAED pattern of as-prepared and sintered NiO NPs: a) as-prepared, b) 350℃ and c) 450℃

It confirms that the particle size grows with increasing annealing temperature. The average particle size of annealed NiO NPs is 28.3 nm at 350℃ and 34.6 nm at 450℃. The SAED pattern validated the crystalline diffraction planes and was well suited to the XRD diffraction patterns of NiO NPs.

3.6 Biocidal activity of NiO NPs

The as-prepared and thermally treated NiO NPs (at temperatures of 350°C and 450°C) are tested for antibacterial efficacy against Gram-positive bacteria (B. subtilis and S. aureus) and Gram-negative bacteria (P. aeruginosa and K. pneumoniae). The obtained zones in agar plates are shown in Figure.8 (a-d). The results of antibacterial activity are summarized as bar diagrams as shown in Figure.9 and are listed in Table 4. As the sintering temperature of the sample is increased, a corresponding reduction in the zone of inhibition is observed. Furthermore, it is evident that bactericidal activity is enhanced with a reduction in particle size, which may be attributable to the increased surface-to-volume ratio. When juxtaposing Gram-positive and Gram-negative bacteria, it has been consistently noted that the sample exhibits a more pronounced antibacterial activity against Gram-negative bacteria compared to Gram-positive bacteria, which may be ascribed to the distinct structural characteristics and thickness of the peptide glycans present in the cell wall. The key reason for the change is due to the fact that sintering provides NiO NPs more crystalline, which enhances their ability to interact with cell membranes. Furthermore, the size of the zone of inhibition was significantly affected by the nanoparticle concentration. Substantial biocidal effects were shown by both as prepared and annealed NiO NPs demonstrating the greater efficacy of the samples. The interaction of NiO NPs with the bacterial cell membrane, which is made up of a lipid bilayer packed with proteins, explains this greater suppression. The process entails NiO NPs producing reactive oxygen species (ROS), which break down the lipid bilayer, oxidatively damaging the membrane and allowing biological components to seep out. Fungal development is ultimately inhibited by this disturbance, which threaten the integrity of the fungal cell membrane. The incorporation of grape juice extract in the synthesis of the NiO NPs is another factor which contributes to the gram positive and gram-negative bacterial effects. The antibacterial characteristics of the nanoparticles may be increased by biologically active compounds found in the grape juice extract, such as the flavonoids, polyphenols, and alkaloids. By interacting with the microbial cell membrane, these chemical compounds may enhance susceptibility which promotes stress caused by oxidation. Additionally, during nanoparticle formation, the grape juice extract functions as a stabilizing and capping agent, which may improve the NiO nanoparticles reactive behaviour and biological compatibility. Prabhu *et al.,* reported that the synthesis of NiO NPs using the flower extract of Clitoriaternatea. Biocidal activity of NiO NPs synthesized using Clitoriaternatea flower extract was systematically examined against E. coli and S. aureus. These NiO NPs are an effective option for application in biomedical field since it is thought that the phytochemical components from the Clitoriaternatea extract present on their surface significantly improve their antibacterial characteristics [26]. It can be clearly observed that the NiO NPs respond through an analogous approach to fighting against bacteria. As a result of the interaction of nanoparticles with the cell wall of the bacteria, ROS are generated and Ni^{2+} ions are released, which may diffuse via the bacterial membrane. Oxidative stress, cellular lipid, amino acid, and damage to DNA, and eventually bacterial cell demise are all effects driven due to generation of ROS and Ni^{2+} ions. A more substantial inhibition zone arises from the improved ROS-generating effectiveness of as prepared NiO nanoparticles due to their size effect [27]. According to the results of antibacterial activity (see Table 4), ROS generation and cellular structure disruption are the main causes of antibacterial and antifungal activity of NiO NPs, the annealing and size distribution of the samples are the key variables in promoting the properties [28-30].

3.7 Anticancer activity

The in vitro cytotoxicity of the green combustion synthesis NiO NPs was evaluated towards A549 cell lines.

Table 4. Bacterial activity of as prepared and annealed NiO NPs against Gram-negative bacteria (*P.Aeruginosa* and *E.Coli*) and Gram-positive bacteria (*B. Subtilis* and *S. Aureus*)

Sample name	Zone of inhibition in diameter (mm)			
	E. Coli	S. Aureas	P. Aeruginosa	B.Substilis
Control	18	17	18	18
As prepared	29	28	29	19
350°C	25	24	27	18
450°C	22	20	23	17

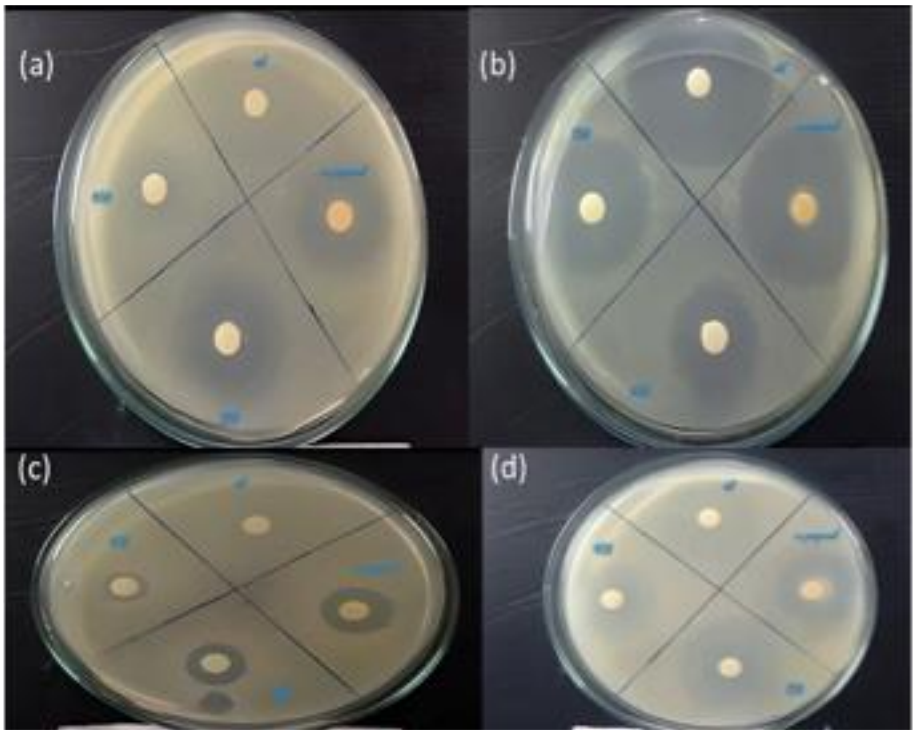

Figure 8. Antibacterial activity of as-prepared and sintered NiO NPs against **(a, d)** Gram-negative bacteria (E.Coli and P.aeruginosa) and **(b, c)** Gram-positive bacteria (S. aureus and B. subtilis)

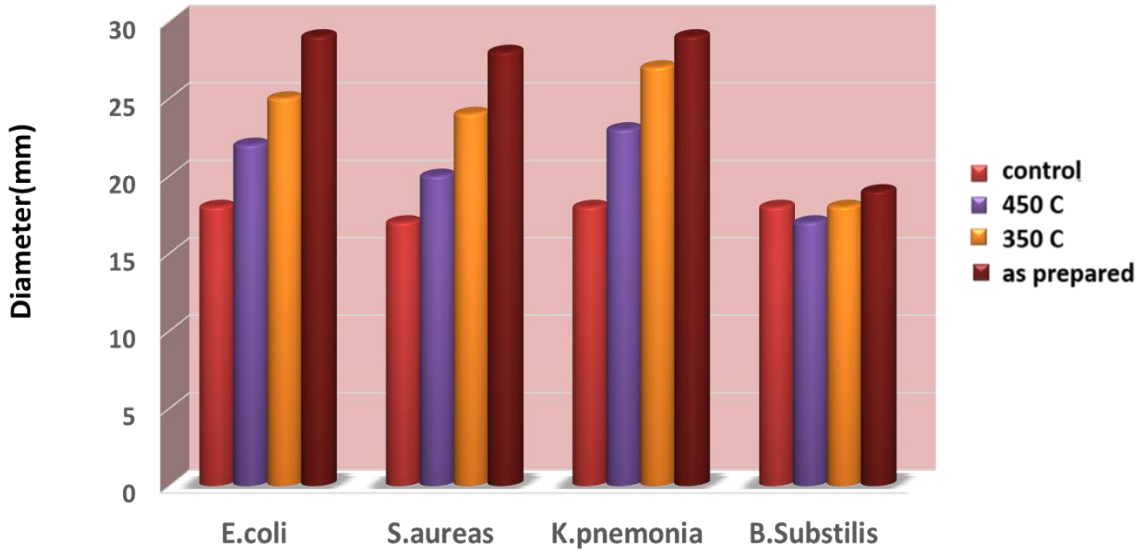

Figure 9. Graphical representation of Zone of Inhibition (mm) of as-prepared and sintered NiO

The cell lines underwent treatment with varying concentrations of the synthesized NiO NPs (control, 10, 25, 50, 75, 100, and 125 µg/ml) over a duration of 24h. Fig.10 illustrates the cytotoxic effects of the biosynthesized NiO NPs on the A549 lung cancer cell line. A maximum cell inhibition rate of 90% was recorded at a concentration of 125 µg/ml. Figure.11 demonstrates that the rate of cytotoxicity against the A549 cell line escalates with an increase in the concentration of the sample, yielding values of 0%, 5%, 17%, 35%, 68%, 79%, and 90%, respectively. The synthesized NiO NPs retain significant organic residues originating from grape juice, encompassing polyphenols, flavonoids, and reducing sugars. These bioactive compounds function as agents for surface capping and stabilization. Notably, they possess the capacity to engage in redox reactions, thereby facilitating enhanced generation of reactive oxygen species (ROS). Deng *et al.* [31], reported that MTE@NiO-NPs, a nickel oxide nanoparticle-decorated extract of Marsdenia tenacissima, showed strong cytotoxicity against A549 and H1299 by causing apoptosis, as shown by the formation of ROS and disruption of mitochondrial membrane.

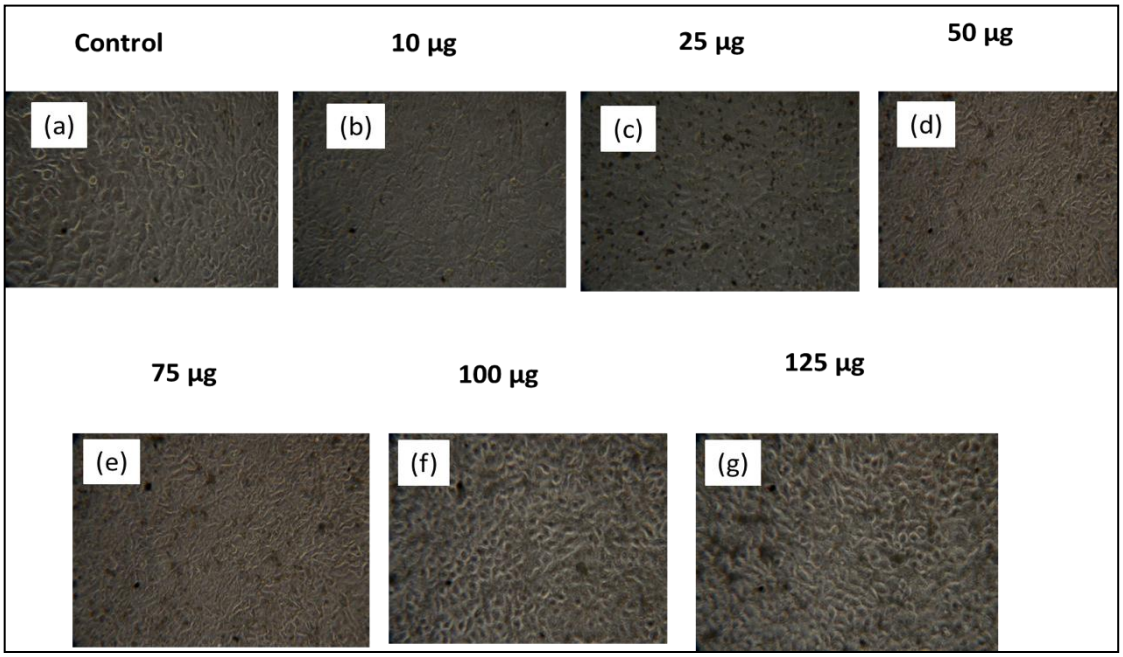

Figure 10. Anticancer activity of as prepared NiO NPs against A549 Cell line

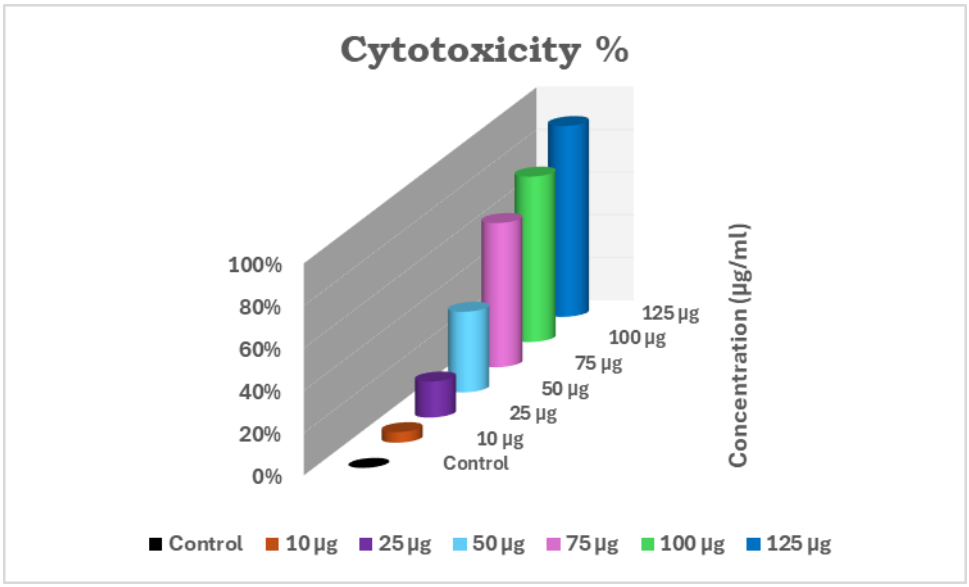

Figure 11. In vitro cytotoxic effect of as prepared NiO nanoparticles (bar diagram)

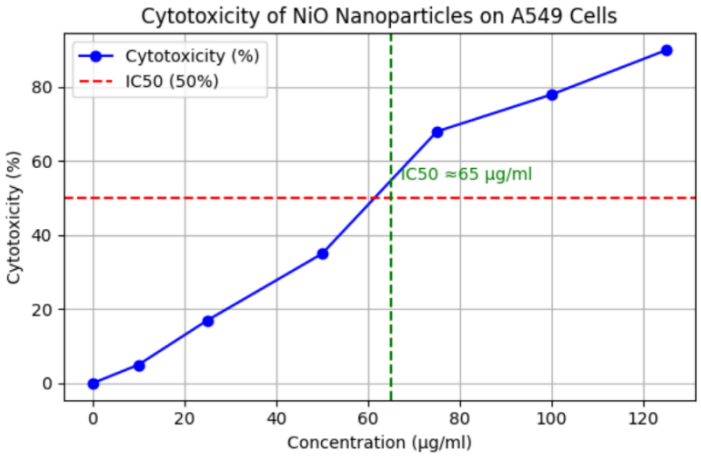

Figure 12. Dose dependent curve to evaluate IC (50) value of as prepared NiO nanoparticles against A549 Cell line.

The dose-response curves pertinent to the A549 cell lines are depicted in Figure.12. The inhibitory concentration $IC_{(50)}$ values for the as prepared NiO NPs against the A549 cell line were determined to be 67 µg/ml. Consequently, in the as-prepared samples, the observed cytotoxicity is attributable to both the inherent properties of NiO and the synergistic effects of residual phytochemicals. Al-Taee *et al.* reported that the biosynthesized nickel oxide nanoparticles (NiO NPs) results in cellular apoptosis by compromising the integrity of the cell membrane. This mechanism is situated within the framework of the mitochondria-dependent intrinsic apoptotic pathway, wherein the interplay between anti-apoptotic and pro-apoptotic proteins ultimately dictates cellular destiny [32].

4. Conclusion

Grape juice successfully used in green combustion technique to synthesis of NiO nanoparticles. It was anticipated that the tartaric acid present in the grape juice provoked the formation of NiO phase while citric acid for Ni phase. The adopted sintering temperatures are not enough to get the complete NiO phase that can be justified from the thermal analysis. The sintering process controlled the agglomeration of nanoparticles due to the initiated caping mechanism of grape juice during the combustion. The elastic parameters revealed the mechanical stability of NiO NPs. The anisotropy factors close to unity confirmed that the samples are exhibiting isotropic elastic behaviour across different processing conditions. The higher value of bulk modulus coupled with consistent rigidity modulus revealed the strong interatomic bonding within the systems. The improvement of biocidal activity was facilitated by the inclusion of biologically active components derived from grape juice extract, highlighting the advantageous outcomes of biosynthesis. Furthermore, the synthesised NiO nanoparticles exhibit in vitro cytotoxic effects on the A549 cell line. This study demonstrates that grape juice-mediated NiO nanoparticles, which integrate an eco-friendly approach with strong antibacterial and anticancer properties, hold considerable potential for biological applications. Their significance in industrial, environmental, and medical fields is clearly demonstrated by the capacity to inhibit microorganism growth.

References

[1] M. Arif, A. Sanger, M. Shkir, A. Singh, R.S. Katiyar, (2019). Influence of interparticle interaction on the structural, optical and magnetic properties of NiO nanoparticles. Physica B: Condensed Matter, 552, 88-95. https://doi.org/10.1016/j.physb.2018.09.023

[2] Y. Wang, S. Bruyère, Y. Kumagai, N. Tsunoda, F. Oba, J. Ghanbaja, H. Sun, J. F. Pierson, (2022). Tuning the optical band gap and electrical properties of NiO thin films by nitrogen doping: a joint experimental and theoretical study. RSC advances, 12(34), 21940-21945. https://doi.org/10.1039/D2RA01887J

[3] W.B. Zhang, N. Yu, W.Y. Yu, B.Y. Tang, Stability and magnetism of vacancy in NiO: a GGA+U study. The European Physical Journal B, 64, (2008)153–158. https://doi.org/10.1140/epjb/e2008-00303-x

[4] A. A. Zaki, T.A. Abdel-Baset, M. Khalafalla, H.A. Qasem, M. Abboudi, F. Al-Wadaani, A.H. Bashal, Nickel Oxide Nanoparticles with and without metallic doping: synthesis structure, conductivity, dielectric, and optical properties. Materials Science and Engineering: B, 291, (2023) 116346. https://doi.org/10.1016/j.mseb.2023.116346

[5] F. Sher, I. Ziani, M. Hameed, S. Ali, J. Sulejmanović, Advanced nanomaterials design and synthesis for accelerating sustainable biofuels production–A Review. Current Opinion in Green and Sustainable Chemistry, 47, (2024) 100925. https://doi.org/10.1016/j.cogsc.2024.100925

[6] S. Wang, D. Chen, Q. Hong, Y. Gui, Y. Cao, G. Ren, Z. Liang, Surface functionalization of metal and metal oxide nanoparticles for dispersion and tribological applications–A review. Journal of Molecular Liquids, 389, (2023) 122821. https://doi.org/10.1016/j.molliq.2023.122821

[7] T. Tamesgen, M.A. Ameya, G. Sisay, L. Yuanqi, Z. Kai, T.T. Beyene, Harnessing the power of S/N-doped NiO nanoparticles through bandgap tuning to achieve enhanced photocatalytic and antibacterial performances. Scientific Reports, 15(1), (2025) 28035. https://doi.org/10.1038/s41598-025-13151-8

[8] K. Ganapathy, S.P. Pandey, S. Bishnoi, J. Suriyaprakash, A.A. Alarfaj, A.H. Hirad, I. Thangavelu, Biocidal activities of nickel oxide nanoparticles modified by copper and manganese, synthesized by green process. Applied Organometallic Chemistry, 38(4), (2024) e7366. https://doi.org/10.1002/aoc.7366

[9] S. Rafiq, M. Aadil, M.F. Warsi, S. Yousaf, M.T. Alotaibi, S.M. El-Bahy, M. Shahid, NiO nanoparticles and their nanohybrid with flat rGO sheets: as an ideal electroactive material for hybrid capacitor applications. Ceramics International, 48(10), (2022) 14596-14605. https://doi.org/10.1016/j.ceramint.2022.01.353

[10] H. Liang, Y. Luo, Y. Xiao, R. Chen, L. Wang, Y. Song, Ni/NiO/carbon derived from covalent organic frameworks for enzymatic-free electrochemical glucose sensor. Ceramics International, 50(1), (2024) 977-984. https://doi.org/10.1016/j.ceramint.2023.10.188

[11] A. Nyabadza, É. McCarthy, M. Makhesana, S.

Heidarinassab, A. Plouze, M. Vazquez, D. Brabazon, A review of physical, chemical and biological synthesis methods of bimetallic nanoparticles and applications in sensing, water treatment, biomedicine, catalysis and hydrogen storage. Advances in Colloid and Interface Science, 321, (2023) 103010. https://doi.org/10.1016/j.cis.2023.103010

[12] B.Y. Hussein, A.M. Mohammed, Biosynthesis and characterization of nickel oxide nanoparticles by using aqueous grape extract and evaluation of their biological applications. Results in Chemistry, 3, (2021) 100142. https://doi.org/10.1016/j.rechem.2021.100142

[13] S. Ramanathan, S. Moorthy, S. Ramasundaram, H.K. Rajan, S. Vishwanath, S. Selvinsimpson, A. Durairaj, B. Kim, S. Vasanthkumar, Grape seed extract assisted synthesis of Dual-Functional anatase TIO2 decorated reduced graphene oxide composite for supercapacitor electrode material and visible light photocatalytic degradation of bromophenol blue dye. ACS Omega, 6(23), (2021) 14734–14747. https://doi.org/10.1021/acsomega.0c02325

[14] C.F. Moreno-Cruz, D. González-Mendoza, U.A. Basilio-Cortes, O. Grimaldo-Juárez, B. Valdez-Salas, E. Beltran-Partida, O. Tzintzun-Camacho, Green synthesis of TiO2 and ZnO nanoparticles using grape pomace extract: characterization and application in cotton fabric. Biocatalysis and Agricultural Biotechnology, 67, (2025) 103645. https://doi.org/10.1016/j.bcab.2025.103645

[15] M. Nawaz, M.B. Tahir, T. Iqbal, M. Pervaiz, M. Rafique, F. Aziz, U. Younas, H. Alrobei, Synthesis, characterization and antibacterial activity of NiO NPs against pathogen. Inorganic Chemistry Communications, 122, (2020) 108300. https://doi.org/10.1016/j.inoche.2020.108300

[16] B. Ahmad, M.I. Khan, M.A. Naeem, A. Alhodaib, M. Fatima, M. Amami, E.A. Al-Abbad, A. Kausar, N. Alwadai, A. Nazir, M. Iqbal, Green synthesis of NiO nanoparticles using Aloe vera gel extract and evaluation of antimicrobial activity. Materials Chemistry and Physics, 288, (2022) 126363. https://doi.org/10.1016/j.matchemphys.2022.126363

[17] S. Sadhukhan, A. Bhattacharyya, D. Rana, T.K. Ghosh, J.T. Orasugh, S. Khatua, K. Acharya, D. Chattopadhyay, Synthesis of RGO/NiO nanocomposites adopting a green approach and its photocatalytic and antibacterial properties. Materials Chemistry and Physics, 247, (2020) 122906. https://doi.org/10.1016/j.matchemphys.2020.122906

[18] A. Haider, M. Ijaz, S. Ali, J. Haider, M. Imran, H. Majeed, I. Shahzadi, M.M. Ali, J.A. Khan, M. Ikram, Green synthesized phytochemically (Zingiber officinale and Allium sativum) reduced nickel oxide nanoparticles confirmed bactericidal and catalytic potential. Nanoscale Research Letters, 15(1), (2020) 50. https://doi.org/10.1186/s11671-020-3283-5

[19] R. Anupriya, V. Kalaiselvi, P. Yasotha, S. Gopi, Sustainable Green Synthesis of ZnO Nanoparticles using Syzygium Cumini Fruit Extract: Structural, Optical, and Antibacterial Investigations. NanoNEXT, 6(4), (2025) 1-9. https://doi.org/10.54392/nnxt2541

[20] M.I.S. Argolo, L.S. Silva, Jr.J.M. Siqueira, F.D.S. Miranda, M.E. Medeiros, F.M. Garrido, Structural and optical properties of Ni/NiO composites synthesized by eco-friendly self-propagation synthesis (SHS): Effects of NH4OH addition. Ceramics International, 45(17), (2019) 21640-21646. https://doi.org/10.1016/j.ceramint.2019.07.161

[21] A.N. Yerpude, V.B. Pawade, S.J. Dhoble, L. Koao, (2023) Lanthanide-doped BaCa2Al8O15 phosphors. Lanthanide-Doped Aluminate Phosphors, 57-80. https://doi.org/10.1016/B978-0-323-90591-6.00003-2

[22] P. Rajkumar, B.K. Sarma, Role of Zn and Mg substitutions on the mechanical behaviour of biomimetic hydroxyapatite and insight of the emergence of hydroxyapatite-ZnO nanocomposite. Materials Characterization, 176, (2021) 111107. https://doi.org/10.1016/j.matchar.2021.111107

[23] S.F. Pugh, Relations between the elastic moduli and the plastic properties of polycrystalline pure metals. The London, Edinburgh, and Dublin Philosophical Magazine and Journal of Science, 45, (1954) 823 – 843. https://doi.org/10.1080/14786440808520496

[24] E. Gobinath, M. Dhatchinamoorthy, P. Saran, D. Vishnu, R. Indumathy, G. Kalaiarasi, Synthesis and characterization of NiO nanoparticles using Sesbania grandiflora flower to evaluate cytotoxicity. Results in Chemistry, 6, (2023) 101043. https://doi.org/10.1016/j.rechem.2023.101043

[25] R.B. da Silva, R.A. Pinto, J.M. Soares, A. Franco, M.A. Correa, F. Bohn, J.A.P. Da Costa, Effect of the synthesis method and calcination temperature on the formation of Ni–NiO nanocomposites. Journal of Sol-Gel Science and Technology, 91, (2019) 286 – 294. https://doi.org/10.1007/s10971-019-05038-8

[26] S. Prabhu, T. Daniel Thangadurai, P. Vijai Bharathy, Pon. Kalugasalam, Synthesis and characterization of nickel oxide nanoparticles using Clitoria ternatea flower extract: Photocatalytic dye degradation under sunlight and antibacterial activity applications. Results in Chemistry, 4, (2022) 100285. https://doi.org/10.1016/j.rechem.2022.100285

[27] P. Ingalagondi, M.S. Sannaikar, K. Mruthunjaya, N. Horti, Optical and antibacterial properties of

nickel oxide (NiO) nanoparticles: Effect of annealing temperature. Results in Surfaces and Interfaces, 19, (2025) 100571. https://doi.org/10.1016/j.rsurfi.2025.100571

[28] R. Kumar, R.S. Gedam, Synthesis and characterization of bi-functional Cu and Ni co-doped ZnO photocatalysts for organic pollutant degradation and antimicrobial activity. Ceramics International, 50, (2024) 24716-24724. https://doi.org/10.1016/j.ceramint.2024.04.208

[29] H. Abbas, M. Mudassar, K. Nadeem, M.T. Yasin, S.A.I. Bokhari, C. Ulrich, The role of Ag ions incorporation on the Magnetic, and Antimicrobial Properties of NiO Nanoparticles. Ceramics International, 50, (2024) 23039-23046. https://doi.org/10.1016/j.ceramint.2024.04.026

[30] A. Khan, M. Shkir, E.H. Ibrahim, M. Kilany, S. AlFaify, M.A. Sayed, A.M. El-Toni, A. Aldalbahi, M.M. Siddiquei, Effect of Bi contents on key physical properties of NiO NPs synthesized by flash combustion process and their cytotoxicity studies for biomedical applications. Ceramics International, 46(12), (2020)19691-19700. https://doi.org/10.1016/j.ceramint.2020.04.047

[31] B. Sun, N. Hu, L. Han, Y. Pi, Y. Gao, K. Chen, Anticancer activity of green synthesised gold nanoparticles from Marsdenia tenacissima inhibits A549 cell proliferation through the apoptotic pathway. Artificial Cells, Nanomedicine, and Biotechnology. 47(1) (2019) 4012-4019. https://doi.org/10.1080/21691401.2019.1575844

[32] M.F. Altaee, L.A. Yaaqoob, Z.K. Kamona, Evaluation of the biological activity of nickel oxide nanoparticles as antibacterial and anticancer agents. Iraqi Journal of Science, 61, (2020) 2888–2896.

Authors Contribution Statement

N. Backiyalakshmi: Conceptualization, Methodology, Validation, Formal analysis, Writing - Original Draft. G. Magesh: Investigation, Data curation. S. Sindhu Kavi: Data curation, Writing - Original Draft. E. Ranjith Kumar: Formal analysis, Writing – Review and Editing, Supervision. M. Deepty: Writing – Review and Editing. Vinayakprasanna N. Hegde: Writing – Review and Editing. G. Venkata Rao: Writing – Review and Editing. Ch. Srinivas: Writing – Review and Editing. A. Ramalingam: Writing – Review and Editing. All the authors read and approved the final version of the manuscript.

Funding

The authors declare that no funds, grants or any other support were received during the preparation of this manuscript.

Competing Interests

The authors declare that there are no conflicts of interest regarding the publication of this manuscript.

Data Availability

The data supporting the findings of this study can be obtained from the corresponding author upon reasonable request.

Has this article screened for similarity?

Yes

About the License